Supplement of Atmos. Chem. Phys., 24, 7467–7479, 2024
https://doi.org/10.5194/acp-24-7467-2024-supplement

Atmospheric Chemistry and Physics Open Access

Supplement of

The role of naphthalene and its derivatives in the formation of secondary organic aerosol in the Yangtze River Delta region, China

Fei Ye et al.

Correspondence to: Jingyi Li (jingyili@nuist.edu.cn) and Jianlin Hu (jianlinhu@nuist.edu.cn)

Contents of this file:

Text S1. Fitting the SOA formation by one-product and two-product methods

In the CMAQ model, counter species were used to calculate the production of SOA through gas-particle partitioning based on yields (α_i) and partitioning coefficients ($K_{\mathrm{om},i}$, m^3 μg^{-1}) of condensable organic products derived from chamber experiment data. The definition of $K_{\mathrm{om},i}$ followed Pankow (1994) as shown below:

$$K_{\mathrm{om},i} = \frac{1}{C^*_{\mathrm{sat},i}} = \frac{RT}{10^6 \overline{\mathrm{MW}_{\mathrm{om}}} \xi_i P^0_{\mathrm{L},i}} \quad (1)$$

where $\overline{\mathrm{MW}_{\mathrm{om}}}$ (g mol^{-1}) is the average molecular weight of the organic phase, ξ_i is the activity coefficient of species *i* in the absorbing organic phase, $P^0_{\mathrm{L},i}$ (atm) is the vapor pressure of species *i* at temperature *T* (K), and *R* (8.314 J mol^{-1} K^{-1}) is the gas constant. Factor 10^6 is needed for unit conversion. The inverse of the saturation concentration of species i, $C^*_{\mathrm{sat},i}$ (μg m^{-3}), is equivalent to $K_{\mathrm{om},i}$. The temperature dependence of $C^*_{\mathrm{sat},i}$ was calculated by the Clausius–Clapeyron equation (Hayes et al., 2015):

$$C^*_{\mathrm{sat},i} = C^*_{0,i} \frac{T_0}{T} \exp\left[\frac{\Delta H_{\mathrm{vap},i}}{R}\left(\frac{1}{T_0} - \frac{1}{T}\right)\right] \quad (2)$$

where $C^*_{0,i}$ is the effective saturation concentration of condensable species *i* at the reference temperature T_0 (K), typically assumed to be 298 K. $\Delta H_{\mathrm{vap},i}$ (J mol^{-1}) is the enthalpy of vaporization.

Assuming that the condensable organic products were P_1, P_2,…P_n, the total SOA yield (*Y*) of a certain parent VOC was calculated as follows (Odum et al., 1996):

$$Y = \sum_i Y_i = M_{\mathrm{o}} \sum_i \frac{\alpha_i K_{\mathrm{om},i}}{1 + M_{\mathrm{o}} K_{\mathrm{om},i}} \quad (3)$$

where α_i is the mass-based stoichiometric coefficient of semi-volatile product *i*. M_o is the total mass concentration of the absorbing aerosol medium. The SOA formation scheme is named the n-product method based on the total number (n) of P_i. Accordingly, the total SOA yield of the two-product and one-product methods can be derived as follows:

$$Y = \frac{\alpha_1}{1 + \frac{1}{M_o K_{om,1}}} + \frac{\alpha_2}{1 + \frac{1}{M_o K_{om,2}}} \quad (4)$$

$$Y = \frac{\alpha_1}{1 + \frac{1}{M_o K_{om,1}}} \quad (5)$$

Text S2. Estimation of Nap and MN emissions

To obtain the detailed emissions of 1-MN and 2-MN, the ratios of 1-MN/2MN to non-methane volatile organic compounds (NMVOCs) of different sources were calculated as follows:

$$p = \sum_{j=1}^{n} (a_j * W_j) \quad (6)$$

where *p* is the mass proportion of 1-MN/2-MN to total NMVOC emissions in a major source, a_j is the mass ratio of 1-MN/2-MN to NMVOCs in a subcategorized source *j*, and W_j is the weight percent of the total emitted NMVOCs from a subcategorized source *j* to that of the major source. For a specific source *j*, a_j was obtained from the U.S. Environmental Protection Agency's (EPA's) repository of organic gas and particulate matter (PM) speciation profiles of air pollution sources (SPECIATEv5.2), and W_j was based on the information reported by An et al. (2021) for the YRD and Li et al. (2014) for other regions, respectively.

Table S1. The yield (α), equilibrium partitioning coefficient (K_{om}), and enthalpy of SOA precursors from Nap, 1-MN, and 2-MN in different scenarios.

	Species	α_1	$K_{om,1}$ (m^3 μg^{-1})	α_2	$K_{om,2}$ (m^3 μg^{-1})	Enthalpy (kJ mol^{-1})	References for α and K_{om}
High NO_x	Nap	0.210	0.602	1.07	3.77E-3	18	CMAQ
(one-product)	1-MN	0.500	0.110	-	-	16.6	Chan et al. (2009)
	2-MN	0.550	0.130	-	-	17.5	Chan et al. (2009)
High NO_x	Nap	0.210	0.602	1.07	3.77E-3	18	CMAQ
(two-product)	1-MN	0.206	0.193	0.107	0.001	16.6	Shakya and Griffin (2010)
	2-MN	0.247	0.193	0.0920	0.001	17.5	Shakya and Griffin (2010)
Low NO_x	Nap	0.730	[a]				CMAQ
	1-MN	0.680	[a]				Chan et al. (2009)
	2-MN	0.580	[a]				Chan et al. (2009)

[a] Constant yield

Table S2. Sector-based mass ratios of Nap, 1-MN, and 2-MN to NMVOC emissions in the emis-orig case.

Emission region	Species	residential	road transport	industry	industrial solvent use	residential solvent use	wildfire[c]
YRD region [a]	Nap	The original Nap emission in YRD					0.391
	1-MN	0.0739	0.0143	2.62E-3	5.47E-4	0.0115	0.134
	2-MN	0.0899	0.0232	0.0116	2.38E-3	0.0500	0.170
	Species	residential	transportation	industry	power	agriculture	wildfire [c]
Other regions [b]	Nap	0.0252	0.0317	0.0983	-	-	0.391
	1-MN	3.95E-3	4.38E-3	1.67E-4	-	-	0.134
	2-MN	0.0108	7.24E-3	1.11E-3	-	-	0.170

[a] The YRD inventory was used for the YRD region and was divided into 13 sources (ship, nonroad transport, road transport, industry, industrial solvent use, residential solvent use, agriculture, residential, industry boiler and kiln, power, dust, oil storage and transportation, gasoline vehicle evaporative emissions), among which only sources with none zero mass ratios of Nap and MN were listed in the Table. [b] The MEIC inventory was used for other regions and was divided into 5 sources. [c] The ratios of Nap and MN for wildfire emissions in the YRD region were the same as in other regions.

Table S3. Model performances of MDA8 O_3 and daily average $PM_{2.5}$, SO_2, NO_2, and CO in several cities listed in Fig. S1 in case-1product. OBS and PRE represent observed and predicted concentrations, respectively. The benchmarks follow Emery et al. (2017). Performances that exceed the benchmark are represented in bold font.

Species	Metrics	Suzhou	Nanjing	Hangzhou	Hefei	Shanghai	Benchmark
MDA8	OBS	68.37	75.22	70.74	71.29	65.85	
O_3 (ppb)	PRE	71.54	71.93	73.49	68.49	47.50	
	NMB	0.05	-0.04	0.04	-0.04	**-0.28**	<±0.15
	NME	**0.25**	0.17	0.22	0.23	**0.33**	<0.25
	r	0.40	0.73	0.62	0.56	0.25	
$PM_{2.5}$	OBS	42.16	38.41	37.65	46.54	42.04	
($\mu g\ m^{-3}$)	PRE	31.83	36.79	31.91	48.53	23.98	
	NMB	-0.24	-0.04	-0.15	0.04	**-0.43**	<±0.30
	NME	0.33	0.26	0.39	0.32	0.47	<0.50
	r	0.36	0.39	0.21	0.38	0.47	
SO_2	OBS	2.33	3.42	3.03	2.50	3.80	
(ppb)	PRE	2.51	3.55	2.36	2.70	1.76	
	NMB	0.08	0.04	-0.22	0.08	-0.54	
	NME	0.35	0.20	0.24	0.36	0.54	
	r	0.49	0.70	0.64	0.50	0.44	
	OBS	18.77	17.84	18.54	19.80	17.34	

NO_2	PRE	12.56	13.84	10.92	15.03	17.57
(ppb)	NMB	-0.33	-0.22	-0.41	-0.24	0.01
	NME	0.34	0.24	0.41	0.25	0.18
	r	0.49	0.67	0.33	0.83	0.83
CO	OBS	549.52	590.07	673.79	644.89	495.34
(ppb)	PRE	471.97	611.71	483.33	507.04	307.43
	NMB	-0.14	0.04	-0.28	-0.21	-0.38
	NME	0.26	0.17	0.30	0.25	0.39
	r	0.73	0.68	0.36	0.50	0.78

Table S4. Model performances of daily ARO1, ARO2MN', BENZ, NO_2, and NO at the Taizhou site in case-1product. The units of OBS (observation) and PRE (prediction) are ppb.

	ARO1	ARO2MN'	BENZ	NO_2	NO
OBS	0.05	0.37	0.52	9.13	1.42
PRE	0.71	0.45	0.61	7.25	0.96
NMB	13.20	0.23	0.19	-0.21	-0.32
NME	13.20	0.36	0.37	0.27	0.62
r	0.80	0.77	0.75	0.79	0.16

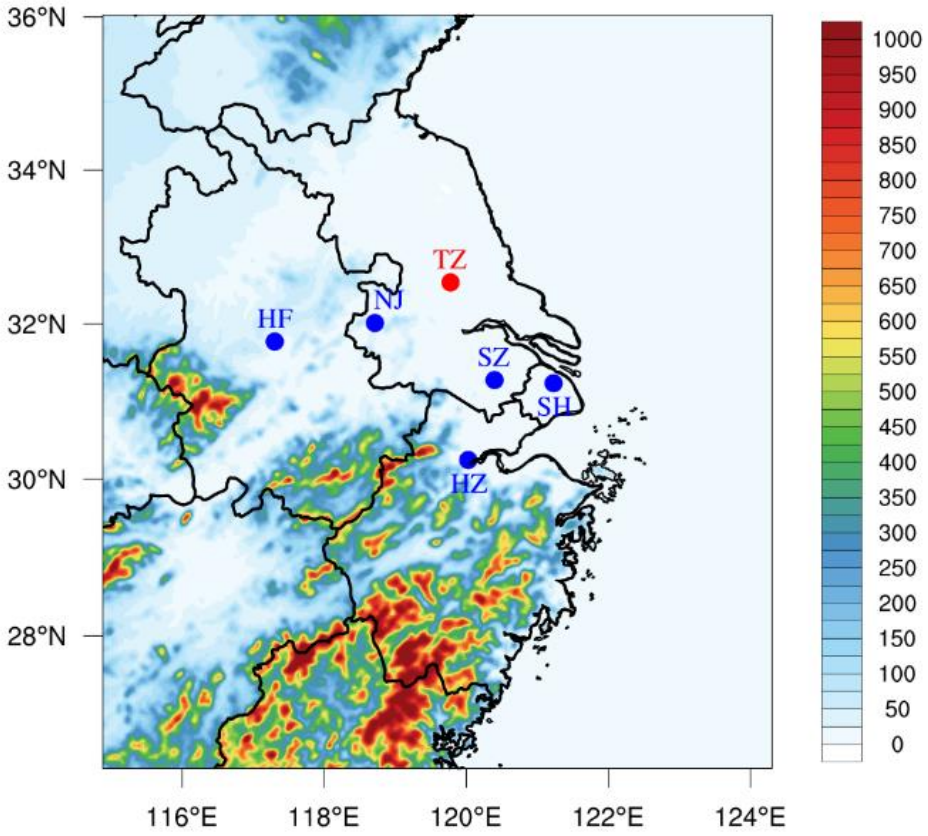

Figure S1. The modeling domain and locations of Taizhou city (red dot) and other sites (Hefei, Nanjing, Suzhou, Shanghai, and Hangzhou; blue dots) for model performance evaluation. The color bar represents the topography height (in meters).

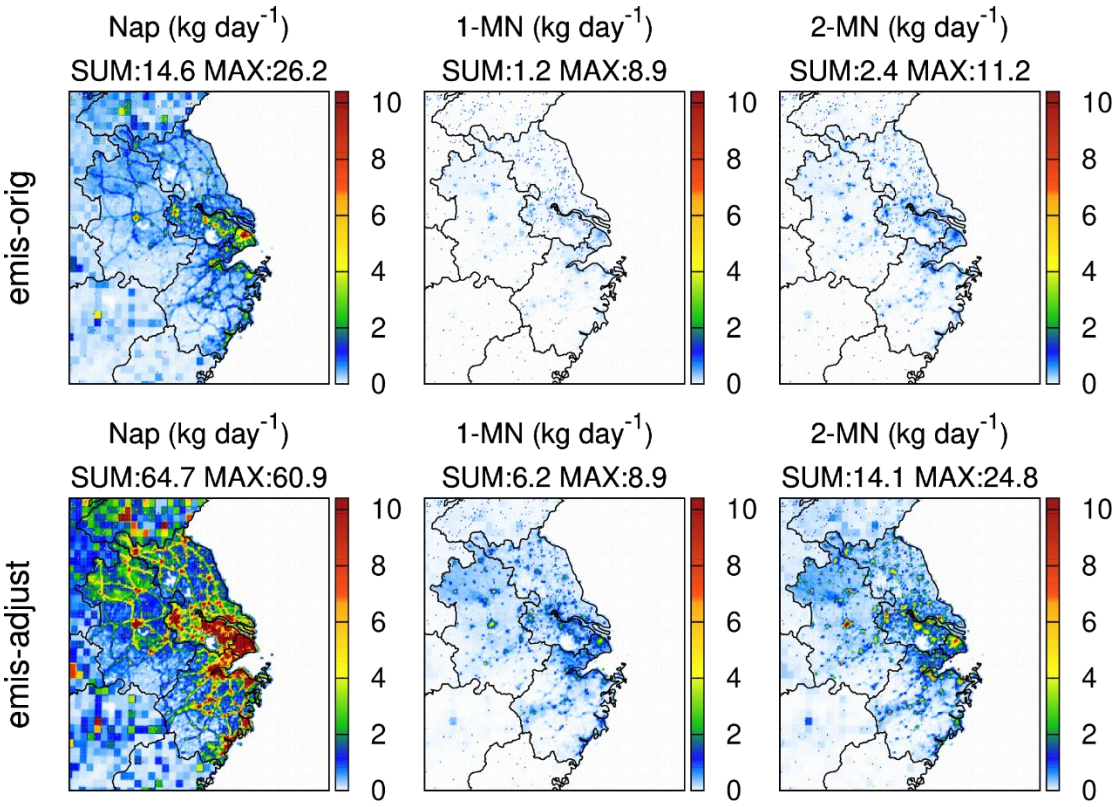

Figure S2. Regional distributions of Nap, 1-MN, and 2-MN emissions in emis-orig and emis-adjust. SUM represents the total emission rate (tons day^{-1}) over the YRD region. MAX represents the maximum emission rate (kg day^{-1}) in the grids of the YRD.

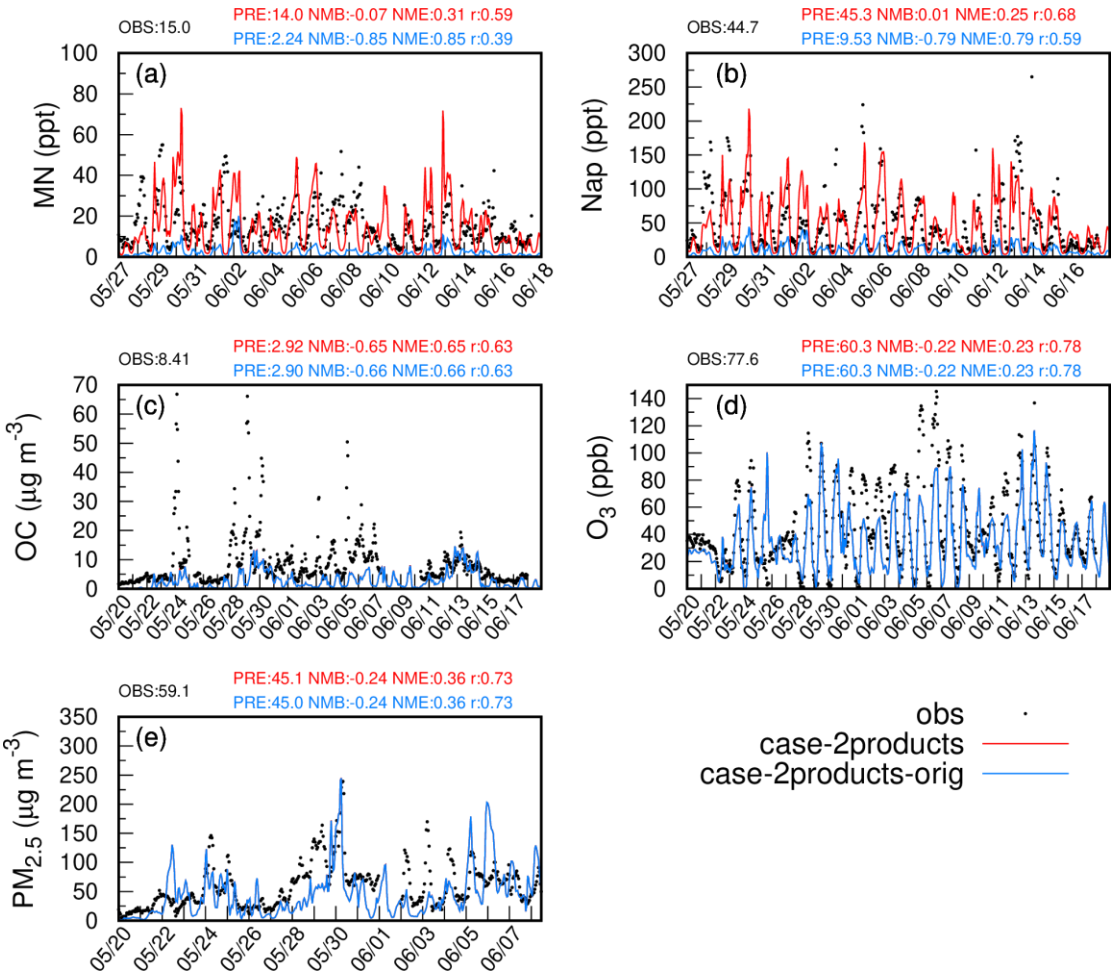

Figure S3. Observed and simulated hourly concentrations of MN, Nap, OC, $PM_{2.5}$, and O_3 based on emis-adjust (red) and emis-orig (blue) at the Taizhou site. Model performances for daily MN, Nap, OC, $PM_{2.5}$, and MDA8 O_3 are shown in blue for case-2products-orig and in red for case-2products. OBS and PRE represent the average of observations and predictions, respectively. Note that the red and blue lines overlap in (c)-(e).

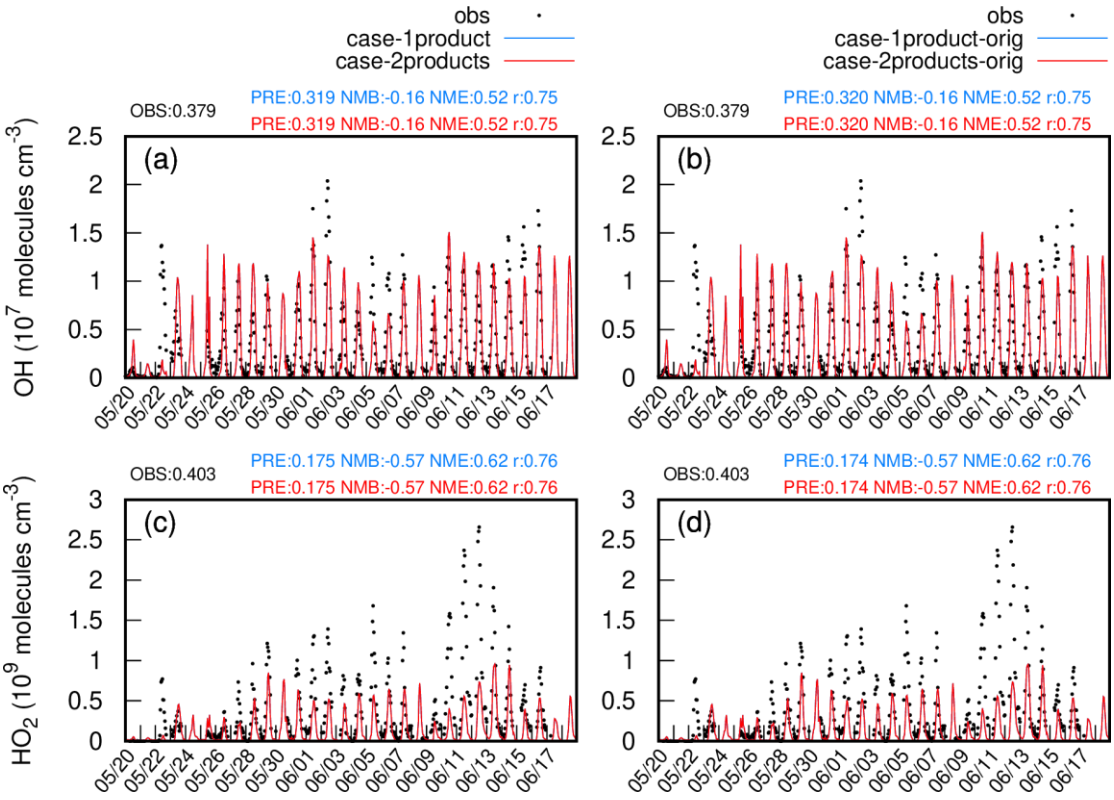

Figure S4. Observed and predicted temporal variations of OH and HO_2 radicals based on emis-adjust (left column) and emis-orig (right column) at the Taizhou site. Model performances for OH and HO_2 radicals are shown in blue for case-1product or case-1product-orig and in red for case-2products or case-2products-orig when compared with the observations from the EXPLORE-YRD campaign. OBS and PRE represent the average of observations and predictions, respectively. Note that the red and blue lines overlap.

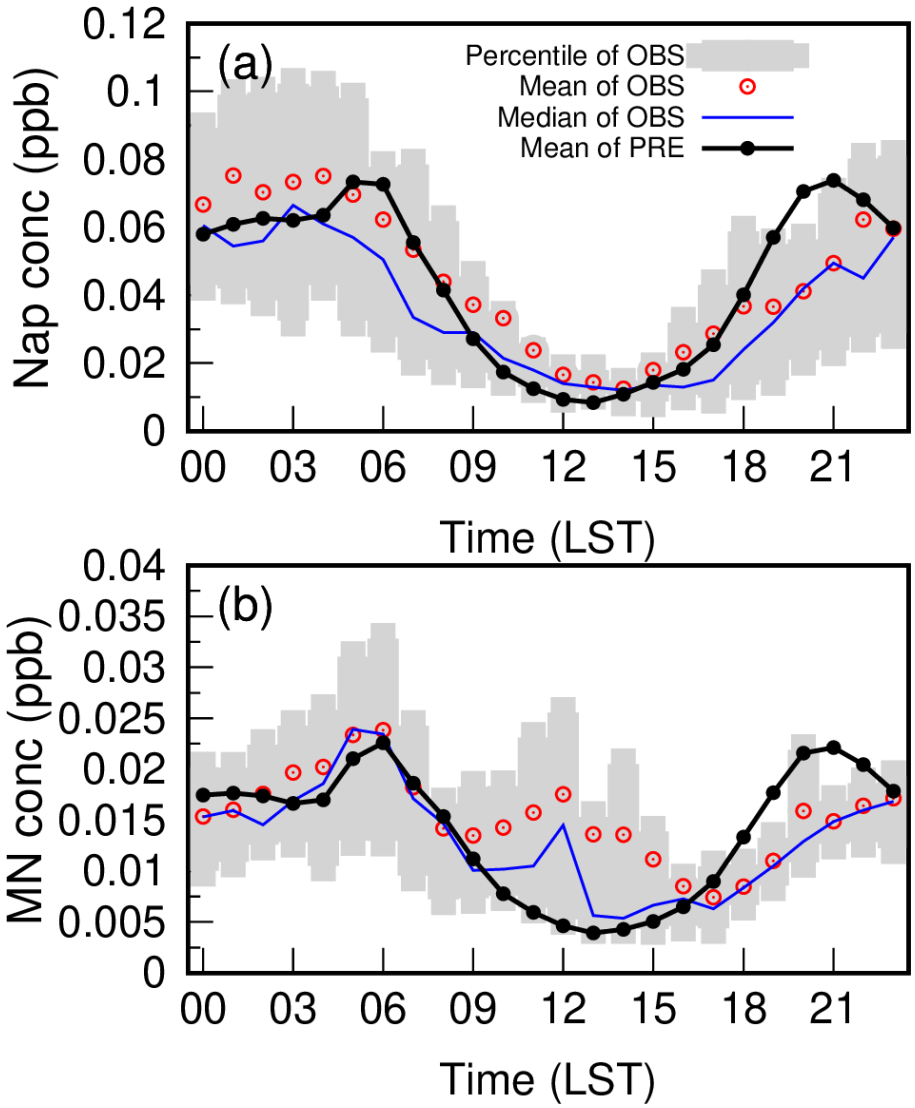

Figure S5. Observed (OBS) and predicted (PRE) diurnal variations of (a) Nap and (b) MN at the Taizhou site. The gray shadow represents the range between the 25th and 75th percentiles of observed concentration.

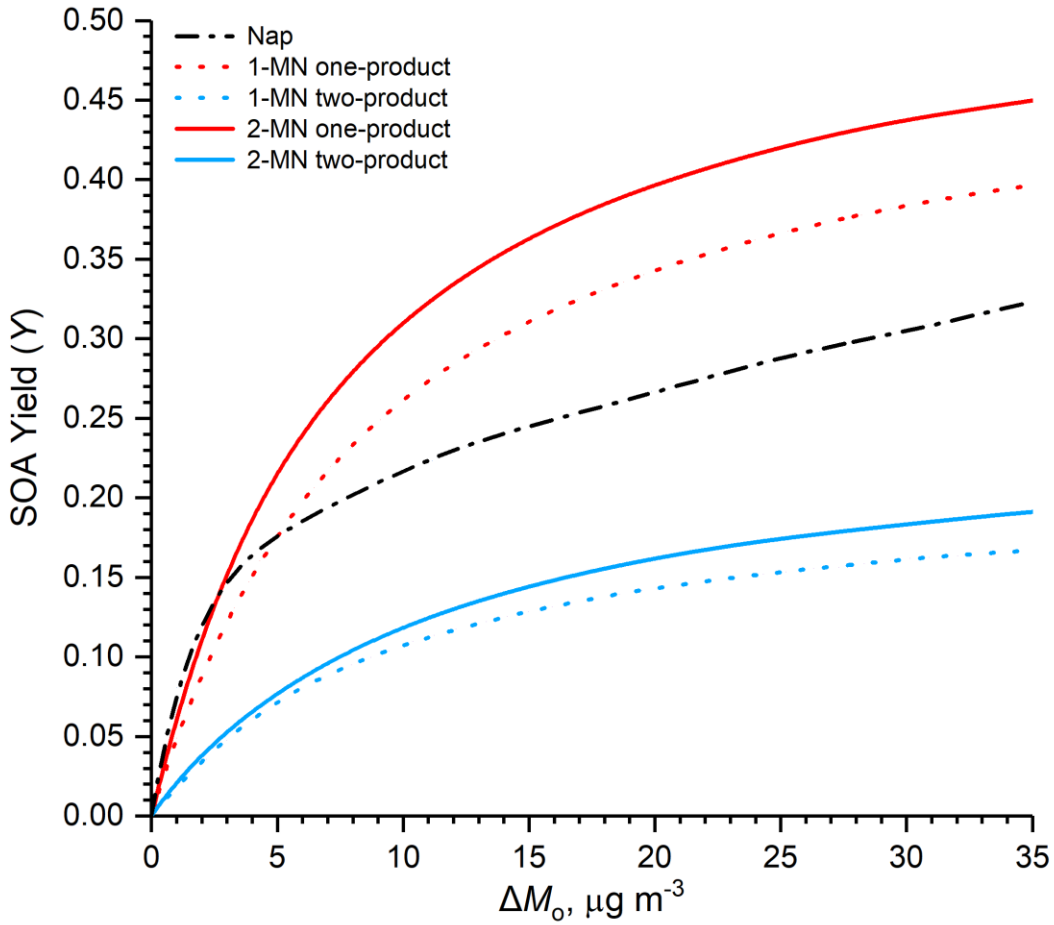

Figure S6. Comparison of fitted SOA yield curves of Nap, 1-MN, and 2-MN under high-NO_x conditions with different total organic mass concentrations (ΔM_o). SOA yield (Y) is calculated as $Y=\Delta M_o \sum_i \frac{\alpha_i K_{om,i}}{1+\Delta M_o K_{om,i}}$, where values of α and K_{om} come from Table S1.

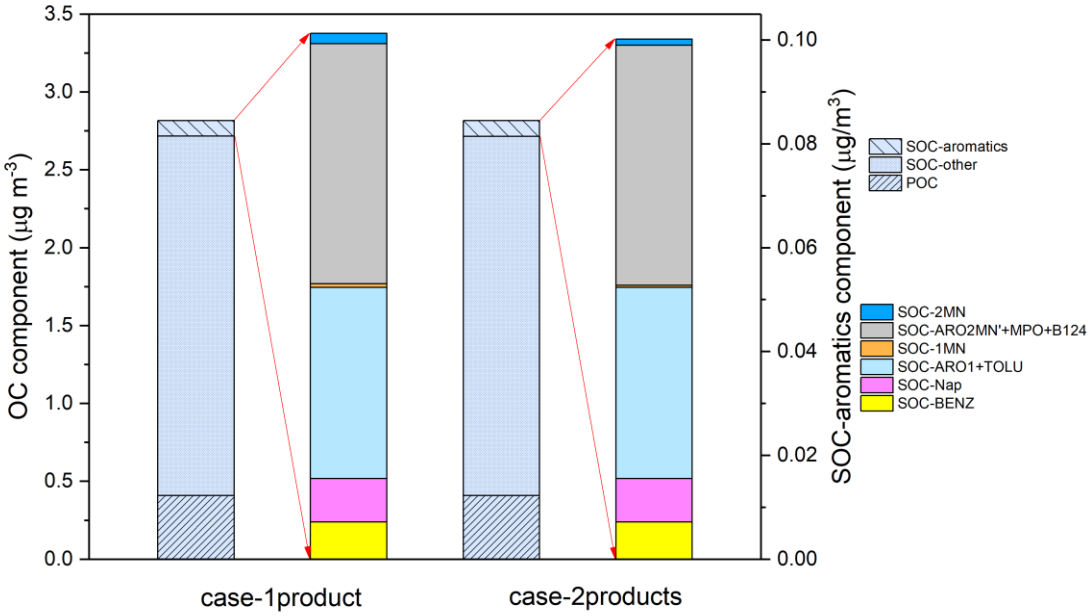

Figure S7. Episode-averaged composition of OC and SOC derived from aromatics in case-1product and case-2products. SOC-aromatics represents the SOC generated by all the aromatic precursors. SOC-other represents SOC minus SOC-aromatics.

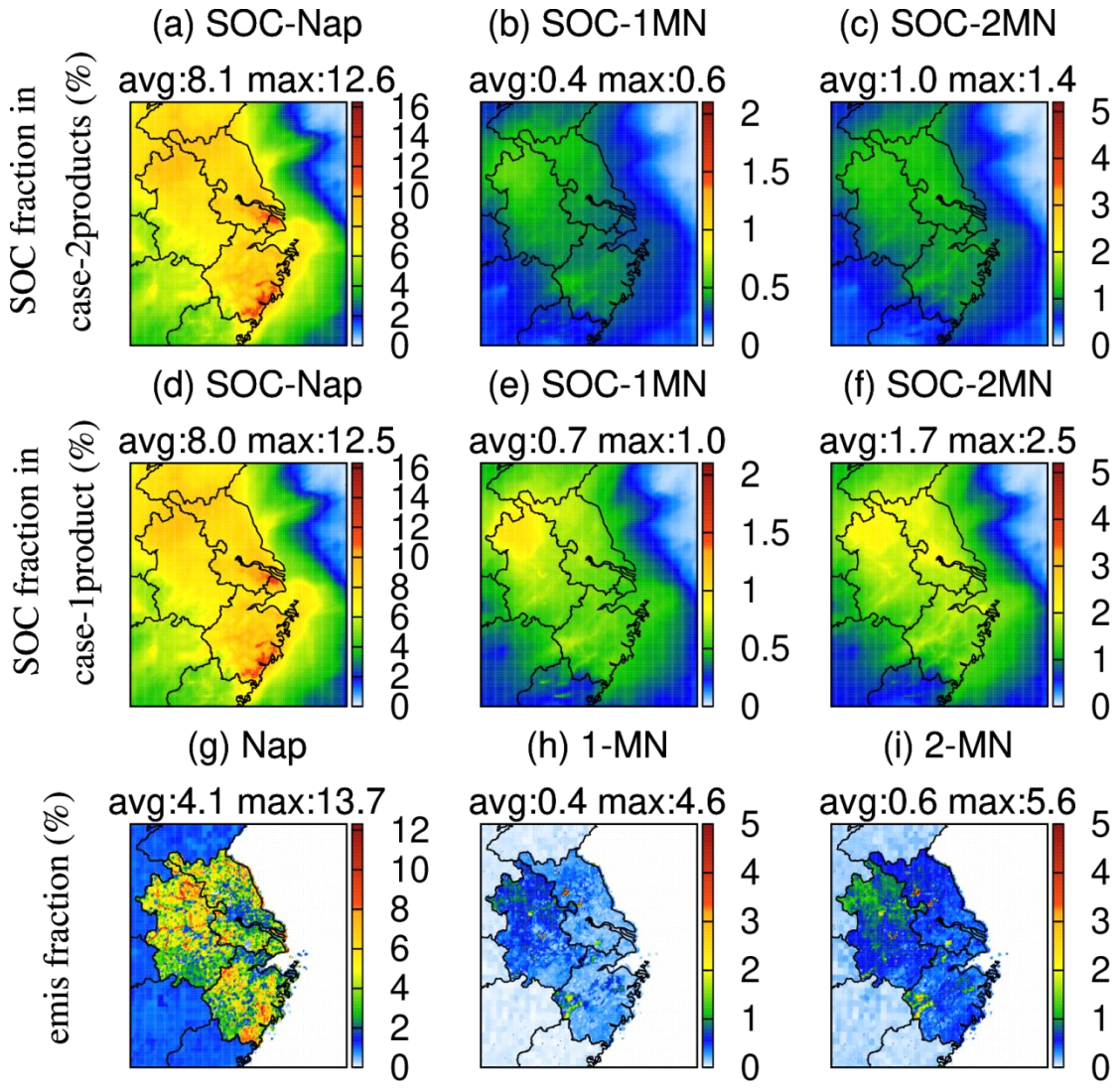

Figure S8. Contributions of Nap, 1-MN, and 2-MN to aromatic-derived SOC in the case-2products (a–c) and the case-1product (d–f) and to the total aromatic emissions (g–i).

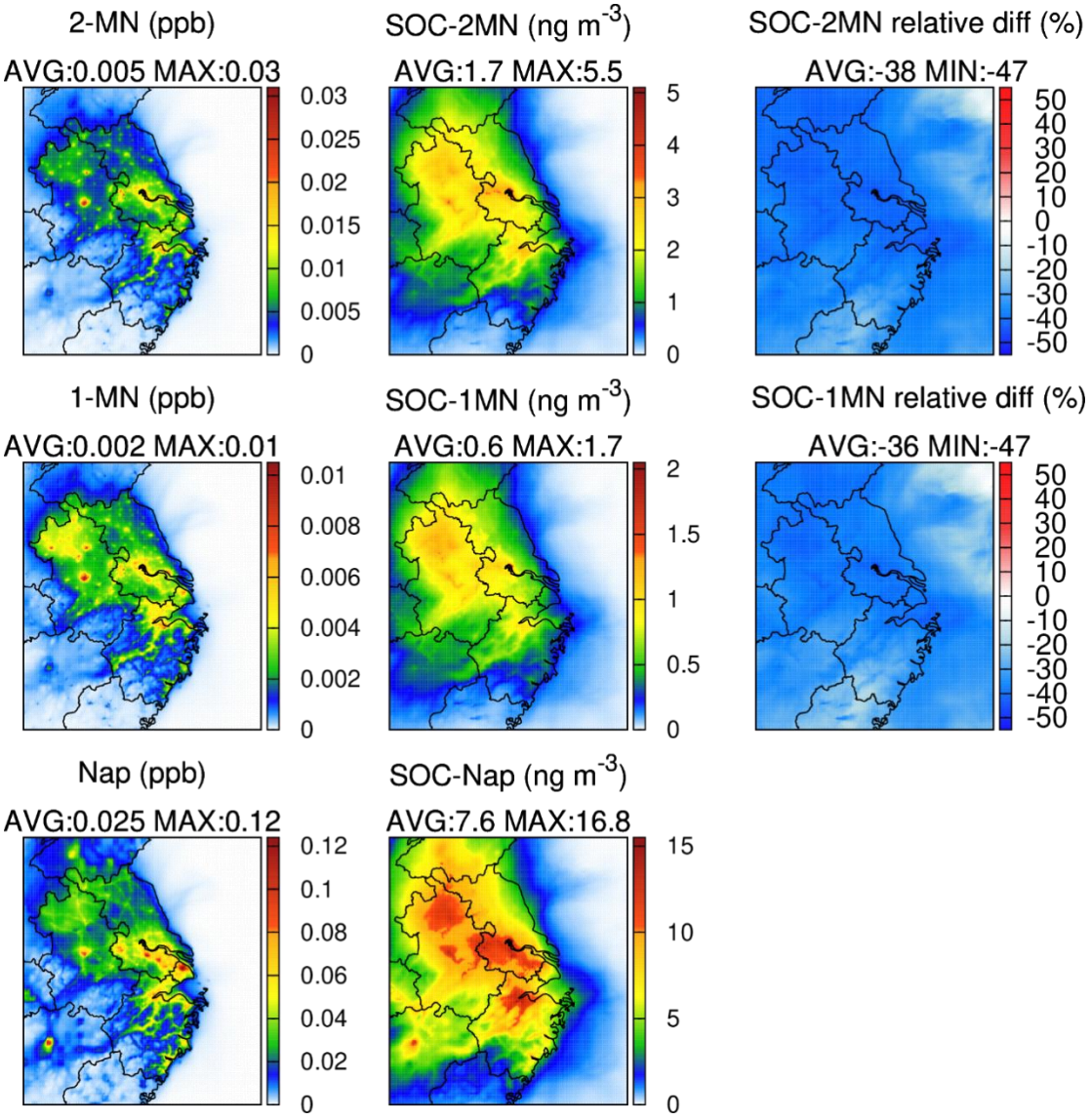

Figure S9. Episode-averaged concentrations of Nap, 1-MN, and 2-MN in case-1product (first column), concentrations of SOC-Nap, SOC-1MN, and SOC-2MN in case-1product (second column), and relative differences in SOC-1MN and SOC-2MN between case-2products and case-1product calculated as (case-2products - case-1product)/ case-1product×100 % (third column).

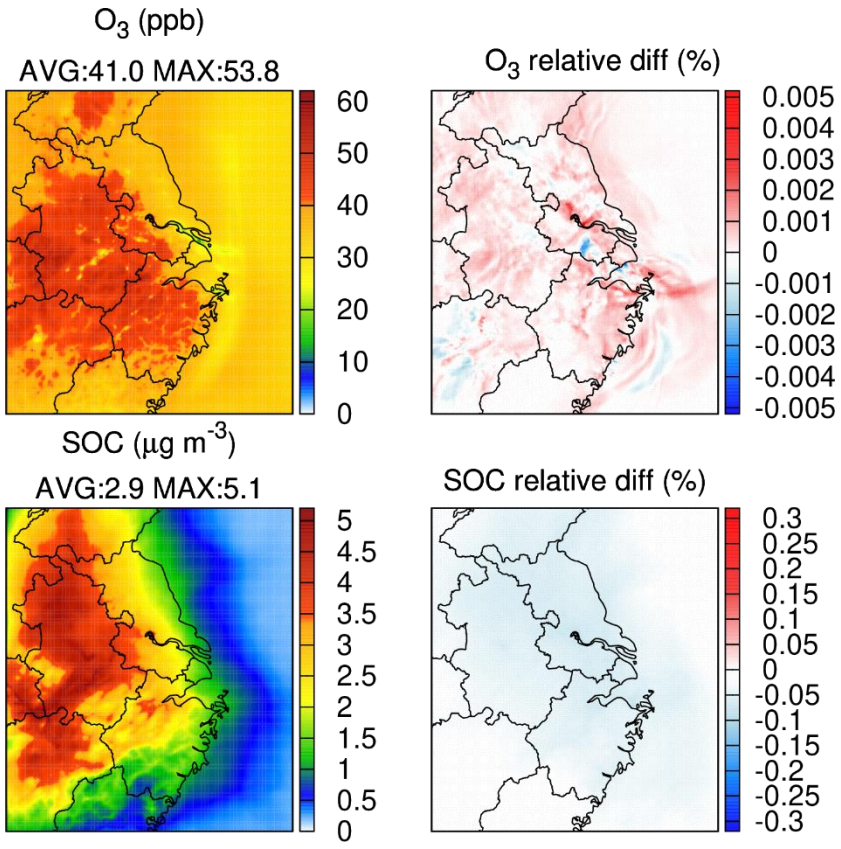

Figure S10. Episode-averaged concentrations of SOC and O_3 in case-1product (left column) and the changes in O_3 and SOC in case-2products relative to case-1product (right column).

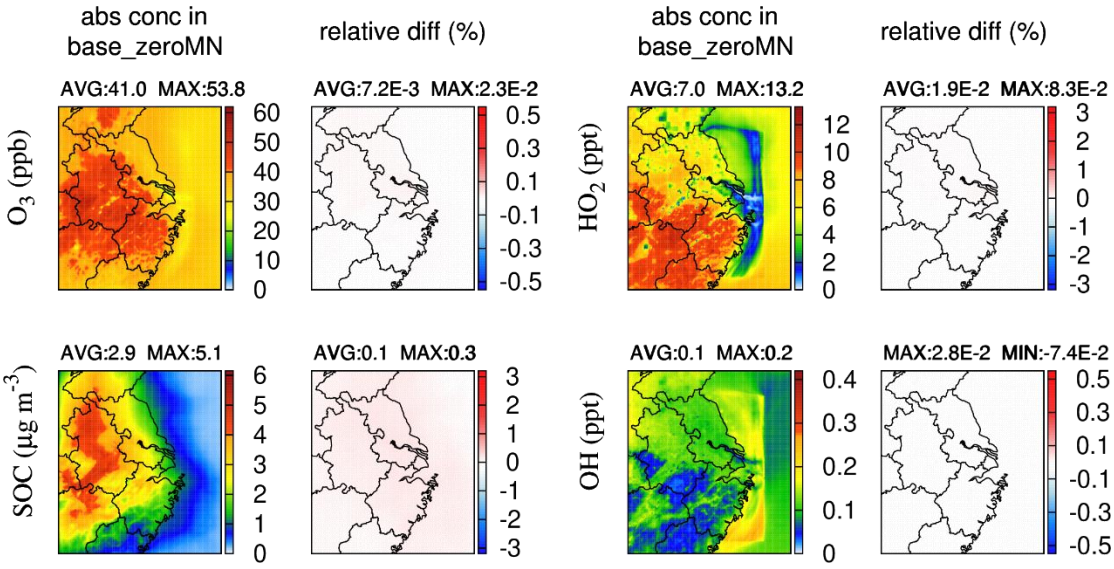

Figure S11. Average concentrations of SOC, O_3, OH·, and HO_2· in base_zeroMN and changes in case-1product relative to base_zeroMN.

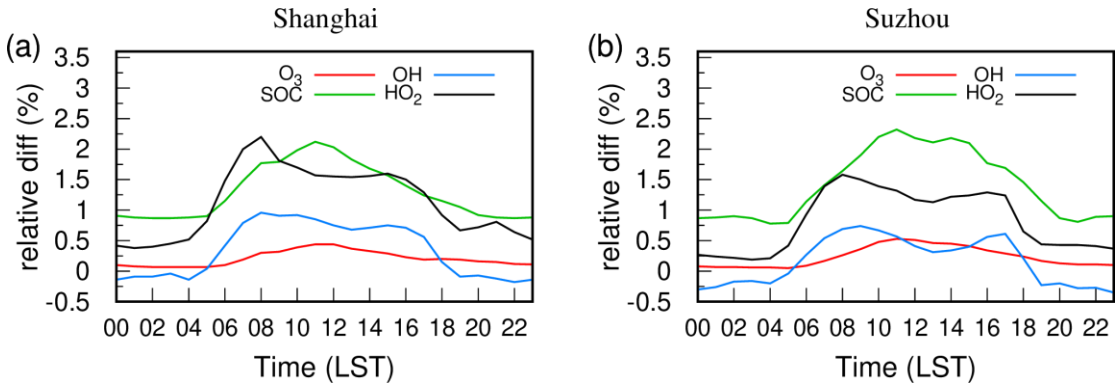

Figure S12. Diurnal relative changes in case-1product compared to base_zeroNapMN in (a) Shanghai and (b) Suzhou.

References

An, J., Huang, Y., Huang, C., Wang, X., Yan, R., Wang, Q., Wang, H., Jing, S. a., Zhang, Y., Liu, Y., Chen, Y., Xu, C., Qiao, L., Zhou, M., Zhu, S., Hu, Q., Lu, J., and Chen, C.: Emission inventory of air pollutants and chemical speciation for specific anthropogenic sources based on local measurements in the Yangtze River Delta region, China, Atmospheric Chemistry and Physics, 21, 2003-2025, 10.5194/acp-21-2003-2021, 2021.

Chan, A. W. H., Kautzman, K. E., Chhabra, P. S., Surratt, J. D., Chan, M. N., Crounse, J. D., Kürten, A., Wennberg, P. O., Flagan, R. C., and Seinfeld, J. H.: Secondary organic aerosol formation from photooxidation of naphthalene and alkylnaphthalenes: implications for oxidation of intermediate volatility organic compounds (IVOCs), Atmospheric Chemistry and Physics, 9, 3049-3060, 10.5194/acp-9-3049-2009, 2009.

Emery, C., Liu, Z., Russell, A. G., Odman, M. T., Yarwood, G., and Kumar, N.: Recommendations on statistics and benchmarks to assess photochemical model performance, Journal of the Air & Waste Management Association, 67, 582-598, 10.1080/10962247.2016.1265027, 2017.

Hayes, P. L., Carlton, A. G., Baker, K. R., Ahmadov, R., Washenfelder, R. A., Alvarez, S., Rappenglück, B., Gilman, J. B., Kuster, W. C., de Gouw, J. A., Zotter, P., Prévôt, A. S. H., Szidat, S., Kleindienst, T. E., Offenberg, J. H., Ma, P. K., and Jimenez, J. L.: Modeling the formation and aging of secondary organic aerosols in Los Angeles during CalNex 2010, Atmospheric Chemistry and Physics, 15, 5773-5801, 10.5194/acp-15-5773-2015, 2015.

Li, M., Zhang, Q., Streets, D. G., He, K. B., Cheng, Y. F., Emmons, L. K., Huo, H., Kang, S. C., Lu, Z., Shao, M., Su, H., Yu, X., and Zhang, Y.: Mapping Asian anthropogenic emissions of non-methane volatile organic compounds to multiple chemical mechanisms, Atmospheric Chemistry and Physics, 14, 5617-5638, 10.5194/acp-14-5617-2014, 2014.

Odum, J. R., Hoffmann, T., Bowman, F., Collins, D., Flagan, R. C., and Seinfeld, J. H.: Gas/Particle Partitioning and Secondary Organic Aerosol Yields, Environmental Science & Technology, 30, 2580-2585, 10.1021/es950943+, 1996.

Pankow, J. F.: An absorption model of gas/particle partitioning of organic compounds in the atmosphere, Atmospheric Environment, 28, 185-188, https://doi.org/10.1016/1352-2310(94)90093-0, 1994.

Shakya, K. M. and Griffin, R. J.: Secondary Organic Aerosol from Photooxidation of Polycyclic Aromatic Hydrocarbons, Environmental Science & Technology, 44, 8134-8139, 10.1021/es1019417, 2010.